RSC Advances

This is an *Accepted Manuscript*, which has been through the Royal Society of Chemistry peer review process and has been accepted for publication.

Accepted Manuscripts are published online shortly after acceptance, before technical editing, formatting and proof reading. Using this free service, authors can make their results available to the community, in citable form, before we publish the edited article. This *Accepted Manuscript* will be replaced by the edited, formatted and paginated article as soon as this is available.

You can find more information about *Accepted Manuscripts* in the Information for Authors.

Please note that technical editing may introduce minor changes to the text and/or graphics, which may alter content. The journal's standard Terms & Conditions and the Ethical guidelines still apply. In no event shall the Royal Society of Chemistry be held responsible for any errors or omissions in this *Accepted Manuscript* or any consequences arising from the use of any information it contains.

ROYAL SOCIETY OF CHEMISTRY

www.rsc.org/advances

Development of non-covalent ternary polymer-CNT composite as a novel supporting material for electrooxidation of glycerol

Dakshinamoorthy Prasanna and Vaithilingam Selvaraj*

Nanotech Research Lab, Department of Chemistry, University College of Engineering Villupuram, (A Constituent College of Anna University, Chennai) Kakuppam, Villupuram-605 103, Tamilnadu, India.

Abstract

The present study is focused on the development of a novel ternary polymer-CNT composite (ATCP-CP-BZD-CNT) by using three different monomers namely amine terminated cyclophosphazene (ATCP), hexachlorocyclotri- phosphazene (CP) and 2,2'-benzidinedisulfonic acid (BZD) as a novel catalyst support for biobased alcohol fuel cell applications. In this regard, Pt and Pt-Sn nanoparticles were deposited on ATCP-CP-BZD-CNT composite material through formaldehyde reduction method using hexachloroplatinic acid hexahydrate and stannous (II) chloride as metal precursor materials. The platinum nanoparticles and platinum-tin loaded ATCP-CP-BZD-CNT composites were characterized by various analytic techniques. The activity and stability of Pt/ATCP-CP-BZD-CNT and Pt-Sn/ATCP-CP-BZD-CNT catalysts were analyzed by cyclic voltammetry and chronoamperometry technique in the presence of 0.5 M glycerol and 0.5 M KOH solution. From the result, it has been concluded that the Pt/ATCP-CP-BZD-CNT and Pt-Sn/ATCP-CP-BZD-CNT electrocatalysts exhibit significant higher anodic oxidation current and lower onset potential when compared to that of Pt loaded vulcan carbon and CNT materials. The various experimental studies demonstrate that the ATCP-CP-BZD-CNT composite shows a huge impact on the physicochemical properties of Pt/ATCP-CP-BZD-CNT and Pt-

RSC Advances Accepted Manuscript

Sn/ATCP-CP-BZD-CNT catalyst for the electrooxidation oxidation of glycerol. Further, the cyclic voltammetry and chronoamperometry analysis of glycerol in alkaline medium concludes that Pt/ATCP-CP-BZD-CNT and Pt-Sn/ATCP-CP-BZD-CNT catalyst is still electroactive even after completion of 100 cycles of various scan potential.

Keywords: Platinum, ternary polymer-CNT composite, carbon nanotubes, glycerol, alcohol fuel cell, electrooxidation

***Corresponding Author:** vaithilingamselvaraj@gmail.com**,** vselva@aucev.edu.in and rajselva_77@yahoo.co.in (V.Selvaraj), **Fax No.** +91-4146 224500

Introduction

Alkaline direct alcohol fuel cells (ADAFCs) are very attractive, renewable and clean energy devices for portable electronics and stationary applications[1]. For direct alcohol fuel cells (DAFCs), glycerol has found to be most sustainable fuel than the methanol and ethanol. Glycerol is glowing for its attractive properties such as low cost, simple purification and storage, non-volatility and environment friendliness, non-toxicity, bio-renewability, a charge capacity of 5.13 Ah m/L and high volumetric energy density of 6.4 kWh/L. [1,2,3] The bio-methanol and bio-ethanol are obtained by the fermentation process of biomass. But, glycerol is frequently obtained as a bio-waste byproduct in the production of biodiesel through a trans-esterification reaction.[4] Glycerol derived from natural oil has found to be low in market price when compared to other alcohols like methanol, ethanol, etc. So, the present work is focused to utilize the biowaste as an alcohol fuel for the generation of electrical energy.

RSC Advances Accepted Manuscript

Carbon nanotubes (CNT) have been exposed much more in the fundamental, theoretical and applied research perspectives because of their extraordinary electrical, mechanical and structural properties.[5,6] In recent years, many efforts have been emphasized for CNT due to their high electrical conductivity, chemical stability and more importantly CNT is working as a support for noble-metal nanoparticle catalysts for fuel cells applications.[7,8] Pristine CNT exhibits poor dispersibility in liquids and agglomerates due to its high surface free energy. Further, the pristine CNT doesn't have sufficient binding sites for the deposition of metal nanoparticles due to their high curvature and chemical inertness.[9] As a result, metal nanoparticles on CNT have poor dispersion and large particle size, which diminishes the electrocatalytic activity. In order to overcome such difficulties, the surface of the pristine CNT is usually modified by harsh acid for functionalization, which cause structural defects and reduces the electrical property of the surface modified CNT.[10,11] So, the recent researches are focused on the development of non-covalent functionalization of CNT using various polymers. The binding between the CNT and polymer is only depend on π-π stacking, hydrogen bonds and van der Waals force of attraction, which will not destruct the structure and electrical properties of CNT.[12,13] However, the reliability of CNT should be maintained because the weak interaction between the polymer and the CNT typically leads to instability of the composites. The instability of the composites is negotiated by introducing polymers with high cross-linked structure and numerous low surface energy groups.[14]

With this view, the present work is proposed to prepare a novel ternary polymer-CNT (ATCP-CP-BZD-CNT) composite through polycondensation method using three different monomers namely amine terminated cyclotriphosphazene (ATCP),

RSC Advances Accepted Manuscript

Hexachlorocyclotriphosphazene (CP) and 2,2'-benzidinedisulfonic acid (BZD). The polymerization process leads to a high cross linked ATCP-CP-BZD ternary polymer formation around the CNT material (core shell structure). To the best of our knowledge, this is the first report involved to synthesize ternary polymer-CNT (ATCP-CP-BZD-CNT) composite using three different monomers like amine terminated cyclotriphosphazene (ATCP), hexachlorocyclotriphosphazene (CP) and 2,2'-benzidinedisulfonic acid (BZD) for biobased fuel cell applications. The whole functionalization is non-covalent, which rarely damage the chemical structure of the carbon nanotubes. As a result, the CNT has been maintained with good electroconductivity and mechanical strength. More importantly, platinum (Pt) and platinum-tin (Pt-Sn) nanoparticles have been successfully deposited on the surface of ATCP-CP-BZD-CNT composites by formaldehyde reduction method[15,16]. The platinum and platinum-tin nanoparticles deposited ATCP-CP-BZD-CNT catalysts were characterized by HRTEM and EDX analyses. The electrocatalytic activity and stability of Pt/ATCP-CP-BZD-CNT and Pt-Sn/ATCP-CP-BZD-CNT electrocatalyst were investigated by using glycerol as a fuel in alkaline medium. The electrocatalysts developed in the present investigation show more enhanced catalytic activity, stability and more negative onset potential, which can be used in alkaline fuel cell applications.

Experimental methods

Materials

Hexachlorocyclotriphosphazene (CP), 2,2'-benzidinedisulfonic acid (BZD), 4-acetamido phenol and multiwalled carbon nanotubes were purchased from Sigma Aldrich, India. Reagent grade formaldehyde (HCHO), triethylamine (TEA), dimethyl sulphoxide

RSC Advances Accepted Manuscript

(DMSO) glycerol and electrocatalyst precursor salt (hexachloroplatinic acid hexahydrate ($H_2PtCl_6 \cdot 6H_2O$) and stannous (II) chloride dihydrate ($SnCl_2.2H_2O$)) were purchased from SRL, India.

Preparation of amine terminated cyclotriphosphazene (ATCP)

A mixture of 4-acetamido phenol (15.65 g, 0.1035 mol) and K_2CO_3 (21.09 g, 0.15824 mol) in dry acetone (200 ml) were effectively agitated at room temperature for 30 minutes. To this mixture, hexachlorocyclotriphosphazene (CP) (5g, 0.0143 mol) was added and refluxed at 60°C for 4 days. Then, the resulted product was cooled to room temperature and filtered. The product (ATCP) was further purified by using hexane and dried in a vacuum oven at 50 °C for 2 h[17-19].

Preparation of ternary polymer-CNT (ATCP-CP-BZD-CNT) composite

In the typical synthesis, 20 mg of hexachlorocyclotriphosphazene, 22.5 mg of 2,2'-benzidinedisulfonic acid (BZD) and 22.5 mg amine terminated cyclophosphazene (ATCP) were dissolved in 80 mL of dimethyl sulfoxide (DMSO). To the above reaction mixture, 5 mg of multiwalled carbon nanotubes was added and dispersed using ultrasonicator for 10 mins. The polymerization of monomers over carbon nanotubes begins with the addition of 2 mL of triethylamine (TEA) into the above dispersion and maintained the ultrasound for 12 hours (100 W, 40 KHz) at room temperature. After that, the resultant precipitate was isolated by the centrifugation process at 3000 rpm for 15 mins, washed three times with DMSO and then distilled water. The resultant ternary polymer-CNT (ATCP-CP-BZD-CNT) composite was dried at 100℃ for 12 hours.

RSC Advances Accepted Manuscript

Synthesis of platinum and platinum-tin nanoparticles deposited ATCP-CP-BZD-CNT composites

Platinum and platinum-tin nanoparticles were deposited on ATCP-CP-BZD-CNT composite by the formaldehyde reduction method according to the **scheme 1**.

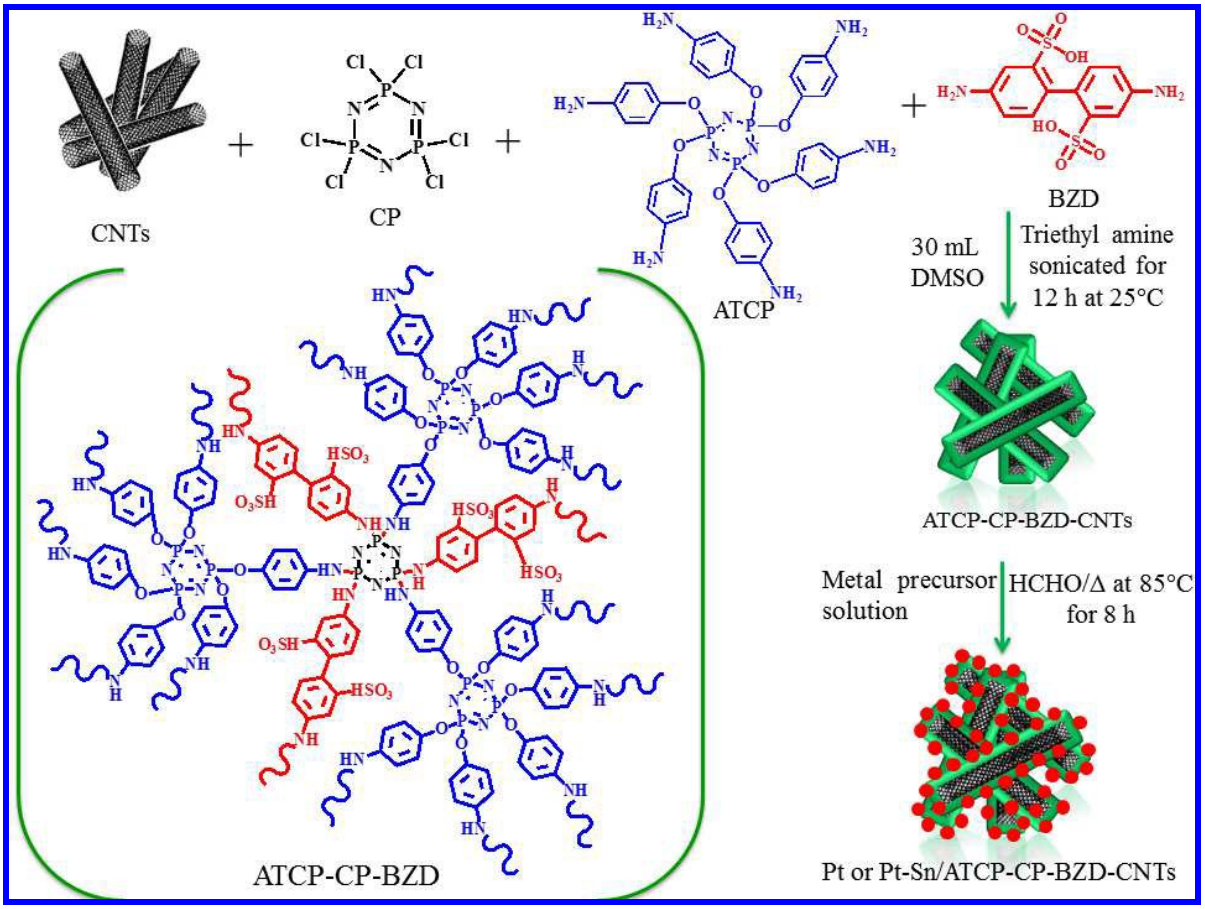

Scheme 1 Schematic representations for the preparation of ATCP-CP-BZD-CNT composite and platinum and platinum-tin nanoparticles deposited ATCP-CP-BZD-CNT composites.

In this process, 30 mg of ATCP-CP-BZD-CNT composite was dispersed in 10 mL of distilled water using ultrasound (100 W, 40 KHz) for 20 mins. Then the platinum precursor solution with a concentration of 54mg/mL was added in dropwise to the above solution and 2.5M NaOH solution was used to adjust the p^H of the reaction mixture (pH=11). Finally,

RSC Advances Accepted Manuscript

platinum nanoparticles were deposited by adding a formaldehyde solution at 85℃ and the reaction was refluxed at the same temperature for 5 hours in an inert atmosphere. After the completion of reduction reaction, the solid Pt/ATCP-CP-BZD-CNT was centrifuged,washed with distilled water and then dried at 60℃ for 10 hours. By using the above process, the Pt-Sn/ATCP-CP-BZD-CNT electrocatalyst was synthesized. The prepared electrocatalysts have been used for the fabrication of electrode towards glycerol fuel cell applications.

Fabrication of Pt/ATCP-CP-BZD-CNT and Pt-Sn/ATCP-CP-BZD-CNT electrodes

The working electrode has been fabricated on graphite electrode through drop casting method. Typically, 5 mg of Pt/ATCP-CP-BZD-CNT electrocatalyst, 100 μL of Nafion solution (5 wt%, Aldrich) and isopropanol (1:1) were mixed using an ultrasonic bath. 25 μL of this mixture was coated on a freshly polished graphite electrode. The electrocatalyst coated graphite electrode was dried at room temperature for 6 hours to remove the solvent like isopropanol. By using the same procedure, the Pt-Sn/ATCP-CP-BZD-CNT has been fabricated and utilized towards the electrooxidation glycerol.

Physicochemical and electrochemical characterizations

The physicochemical characterizations were carried out by using FTIR, HRTEM and EDX analysis. The prepared ATCP-CP-BZD-CNT composite has been examined by fourier transform infrared (FTIR, Thermo Nicolet Model: 6700) technique. The surface morphology and size of metal nanoparticles deposited on ATCP-CP-BZD-CNT composite were analysed by high resolution transmission electron microscope (HR-TEM, JEOL) with an accelerating voltage of 120 kV. Energy dispersive X-ray analysis (EDX, INCA200) confirms the presence of platinum and platinum-tin nanoparticles on ATCP-CP-BZD-CNT composite.

RSC Advances Accepted Manuscript

The electrochemical characterizations were carried out using a multichannel electrochemical workstation with inbuilt FRA system (Biologic SAS, Model VSP2). A standard three-electrode glass cell equipped with novel modified graphite electrodes as working, saturated calomel electrode as reference and a Pt wire as counter electrode were employed. Further, the electrocatalytic activity of glycerol oxidation has been investigated in 0.5 M KOH and 0.5 M glycerol solution with a potential range of -1.0 to 0.3 V at a scan rate of 20, 50 and 100 mVs^{-1}.

The intermediate products formed during the glycerol electrooxidation were determined by using high-performance liquid chromatography (Dionex system P680 HPLC). It works with an isocratic elution and mainly includes an autosampler (ASI 100 Automated Sample Injector), a sample loop (20 μL), and an ion-exclusion column (Aminex HPX-87H), which were operated at room temperature. The analytes were separated with diluted sulfuric acid (3.3 mmol L^{-1} H_2SO_4, MERCK 96%) used as eluent with a 0.6 mL min^{-1} flow rate. The chromatograph was equipped with an UV−Vis detector (λ = 210 nm) followed by a refractive index detector (IOTA2).

Results and discussions

FTIR analysis of amine terminated cyclotriphosphazene (ATCP)

Figure 1 shows the FT-IR spectrum of amine terminated cyclotriphosphazene. The two broad band's observed at 3438 and 3338 cm^{-1} were corresponding to -NH_2 stretching vibrations, in fact they are also ascertain the presence of the amine group in the ATCP material (**Figure 1**). The peaks observed at 3043 and 2925 cm^{-1} were corresponding to ring C-H stretching vibrations. The aromatic C-C stretching vibrations were noticed at 1507 and 1621 cm^{-1}. The characteristic stretching vibrations of P-O-Ph, P-N-P and P-O-C were

RSC Advances Accepted Manuscript

visualized at 1256, 1178 and 952 cm^{-1}, respectively. The aromatic C-H bending vibrations were appeared at 832 and 695 cm^{-1}.

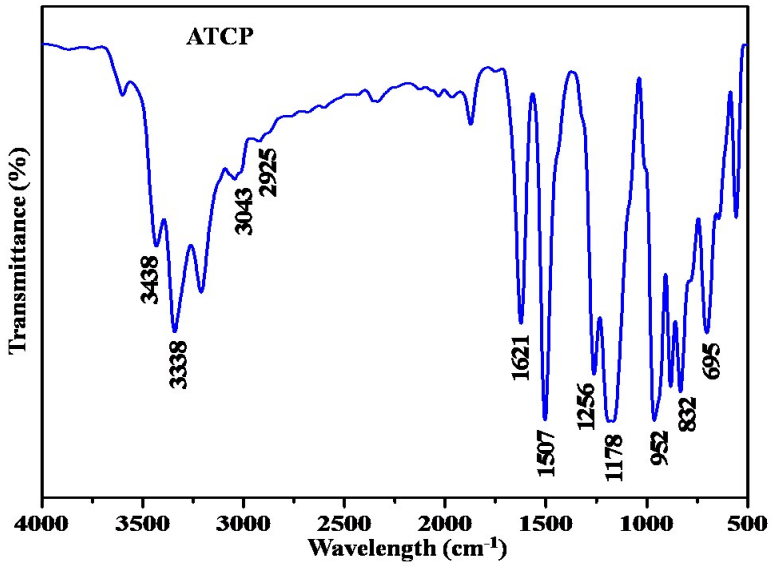

Figure 1 FT-IR spectrum of amine terminated cyclophosphazene (ATCP).

FTIR analysis of ATCP-CP-BZD and ATCP-CP-BZD-CNT materials

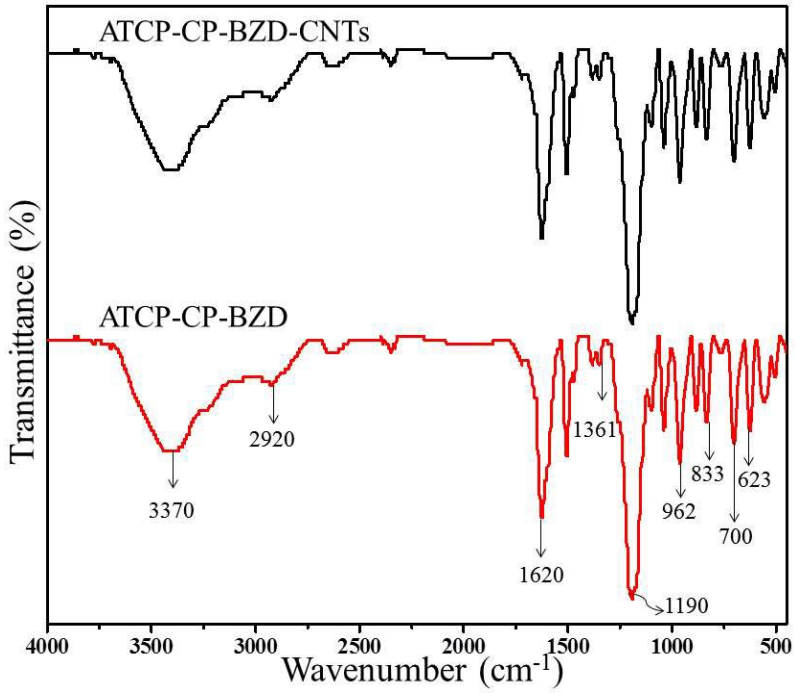

Figure 2 FTIR spectra of ATCP-CP-BZD and ATCP-CP-BZD-CNT materials

RSC Advances Accepted Manuscript

Figure 2 shows the FTIR spectra of ATCP-CP-BZD and ATCP-CP-BZD-CNT materials. From the FTIR spectrum of ATCP-CP-BZD material, the characteristic peaks of -N-H, C-H, C=C, P-O-C, P-N-P, P-O-C and C-S were observed at 3370 cm^{-1}, 2920 cm^{-1}, 1620 cm^{-1}, 1361 cm^{-1}, 1190 cm^{-1}, 695 cm^{-1} and 623 cm^{-1} which indicates the existence of ATCP and BZD in ATCP-CP-BZD material. Furthermore, importantly the P–NH–(Ph) peak at 962 cm^{-1} representing the link formation of the CP with ATCP and BZD. Thus the above discussion can reasonably ascertain the polymerization between CP, ATCP and BZD through the polycondensation process. FTIR spectrum of ATCP-CP-BZD-CNT composite has all the characteristic stretching vibration that was observed as in the case of ATCP-CP-BZD materials, which confirm the existence of ATCP-CP-BZD material on the surface of the CNT. The above analysis can make a conclusion that the ATCP-CP-BZD-CNT contain the structural unit of amine terminated cyclotriphosphazene, 2,2'-benzidinedisulfonic acid and hexachlorocyclotriphosphazene.

XRD analysis

The XRD analyses were carried out for CNT, ATCP-CP-BZD and ATCP-CP-BZD-CNT materials (**Figure 3**). The characteristic peaks of the CNT were observed at 25.53° and 41.01° for 002 and 100 diffraction plane of carbon in CNT. A broad peak was observed between 5 and 15° in the case of ATCP-CP-BZD material, which confirms the amorphous nature of the resultant ATCP-CP-BZD material. The above characteristic peaks of CNT and ATCP-CP-BZD were appeared in the XRD spectrum of ATCP-CP-BZD-CNT composite, which confirms the existence of ATCP-CP-BZD on the surface of CNT material.

RSC Advances Accepted Manuscript

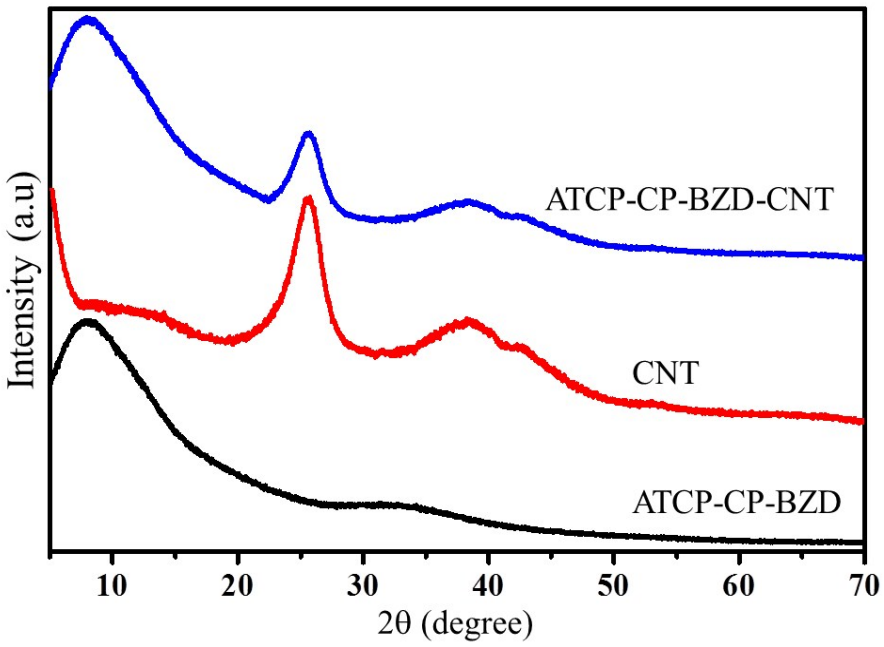

Figure 3 X-ray diffraction patterns of ATCP-CP-BZD-CNT, CNT and ATCP-CP-BZD materials

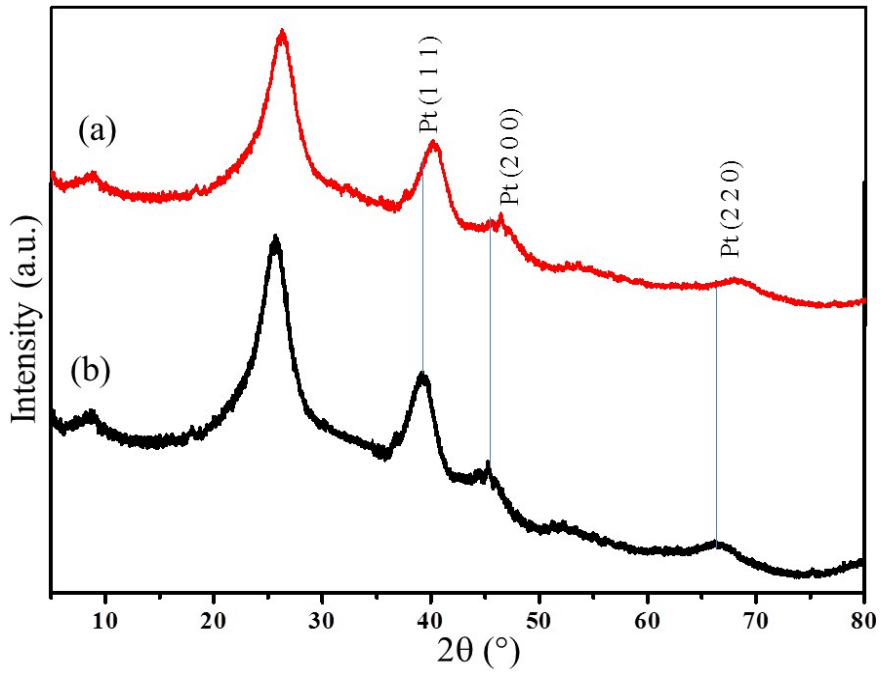

Figure 4 X-ray diffraction patterns of Pt/ATCP-CP-BZD-CNT and Pt-Sn/ATCP-CP-BZD-CNT electrocatalyst

RSC Advances Accepted Manuscript

From the XRD patterns of Pt/ATCP-CP-BZD-CNT and Pt-Sn/ATCP-CP-BZD-CNT (**Figure 4**), the diffraction pattern that is corresponding to the fcc structure of Pt nanoparticles were observed at the Bragg angles (2θ) of 39.44°, 45.08° and 66.98° for the diffraction planes (111), (200) and (220) along with the characteristic peak of ATCP-CP-BZD and CNT. Similar XRD patterns were also observed for Pt-Sn/ATCP-CP-BZD as in the case of Pt/ATCP-CP-BZD-CNT and the peaks were located at higher 2θ value when compared to that of the Pt/PCFA-CNT material, which indicates the formation of Pt-Sn alloy on the surface of ATCP-CP-BZD-CNT material. However, the peak intensity corresponding to ATCP-CP-BZD was decreased, which confirms the presence of Pt and Pt-Sn nanoparticles on the ATCP-CP-BZD but not on CNT. Further, the average particle size of Pt and Pt-Sn nanoparticels were calculated by using Scherrer equation[20] are 2.4 and 2.6 nm, respectively.

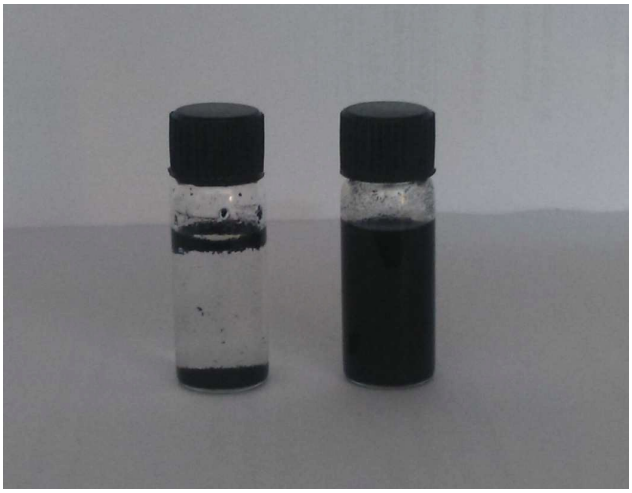

Figure 5 Optical images of CNT (left) and ATCP-CP-BZD-CNT (right) materials dispersed in water.

Further the cross linking density and core shell formation was confirmed by the simple dispersion method as per the previous method.[14] **Figure 5** shows the optical images

RSC Advances Accepted Manuscript

of CNT and ATCP-CP-BZD-CNT dispersion in water. From the **Figure 5**, it was visualized that the CNT displays poor dispersion in water compared to ATCP-CP-BZD-CNT composites because of its high surface free energy. But, non-covalent functionalized ATCP-CP-BZD-CNT composite with highly cross-linked structure, numerous low surface energy–HSO_3 and -NH groups on its surface can greatly improve the dispersibility of CNT material. Based on these results, it was concluded that the CNT was fully covered by ATCP-CP-BZD through cross-linked core structure (**Figure 5)** as shown in the **Scheme 1.**

X-ray photoelectron spectroscopy

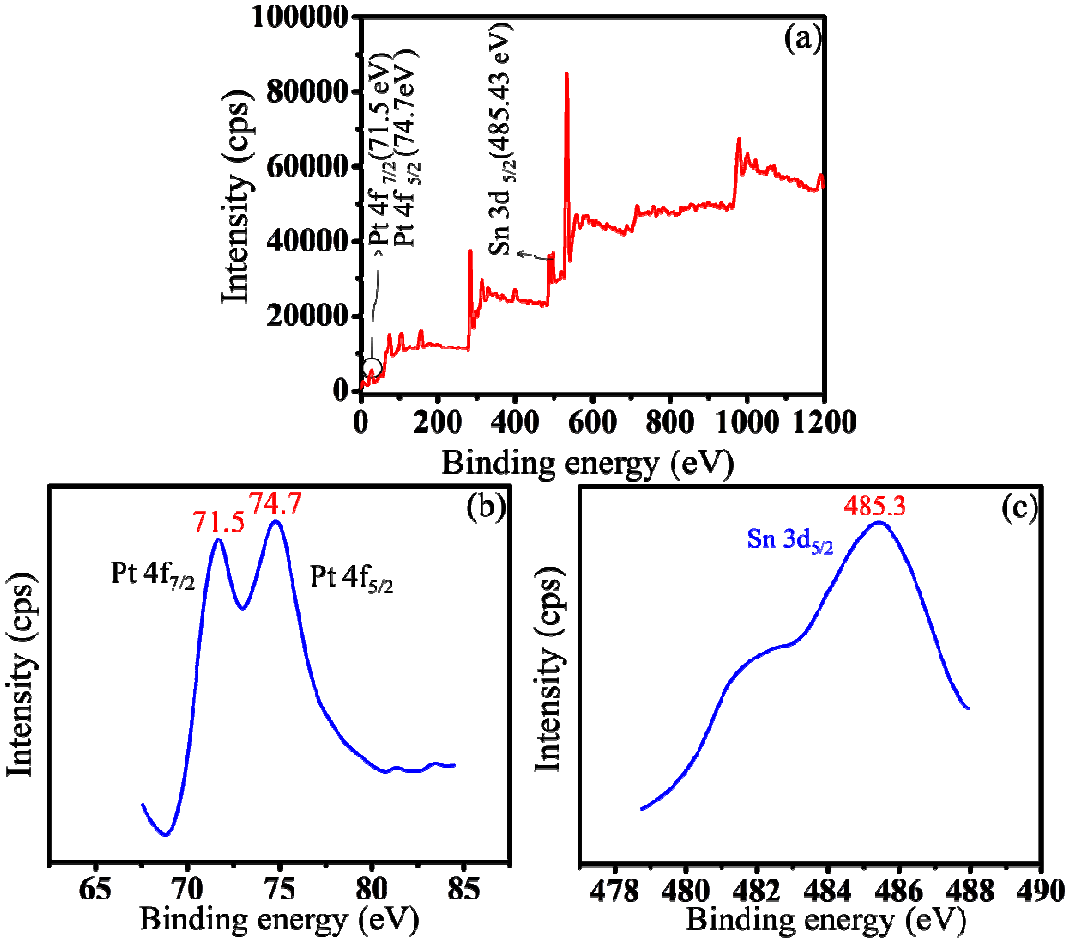

Figure 6 (a) XPS full scan spectrum of Pt-Sn/ATCP-CP-BZD-CNT and XPS spectra of (b) Pt 4f peak (c) Sn 3d peak in Pt-Sn/ATCP-CP-BZD-CNT catalyst.

RSC Advances Accepted Manuscript

XPS analysis was carried out to determine the chemical state of individual metal present in Pt-Sn/ATCP-CP-BZD-CNT catalyst. **Figure 6** shows the XPS spectrum of Pt-Sn/ATCP-CP-BZD-CNT catalyst. The full scan XPS spectrum also confirms the presence of Pt and Sn in the Pt-Sn/ATCP-CP-BZD-CNT catalyst. The images in the **Figure 6 (b & c)** show the XPS spectra of Pt(4f) and Sn(3d) in Pt-Sn/ATCP-CP-BZD-CNT catalyst. The binding energy values of Pt($4f_{7/2}$) and Pt($4f_{5/2}$) are 71.5 and 74.7 eV, respectively. These observed binding energy values are good concords with the literature values of 71.2 and 74.4 eV, which authenticate that the Pt is in the zero valence state. [21, 22] The binding energy value of Sn($3d_{5/2}$) is 485.4 eV, which is also confirming that the Sn is in the zero valence state.[23]

High resolution transmission electron microscopy

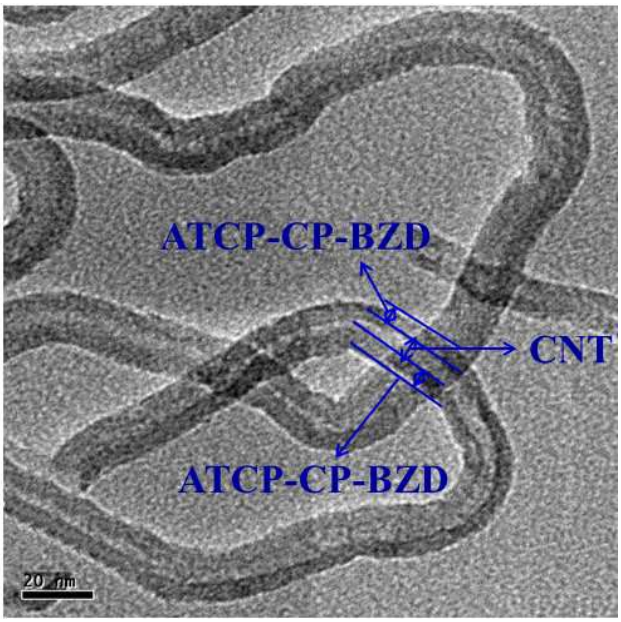

Figure 7 TEM Images of ATCP-CP-BZD -CNT composites

Figure 7 shows the TEM image of ATCP-CP-BZD-CNT composite material. The core-shell structure of ATCP-CP-BZD-CNT composite was clearly visualized from

RSC Advances Accepted Manuscript

HRTEM image of ATCP-CP-BZD-CNT material. From the **Figure 7**, it could be seen that the ATCP-CP-BZD was uniformly coated on CNT with the shell thickness in the range of 3-5 nm. Further, it was also noticed that the surface of the CNT is almost covered by the ATCP-CP-BZD material, which was in good accord with the previous report [14,24].

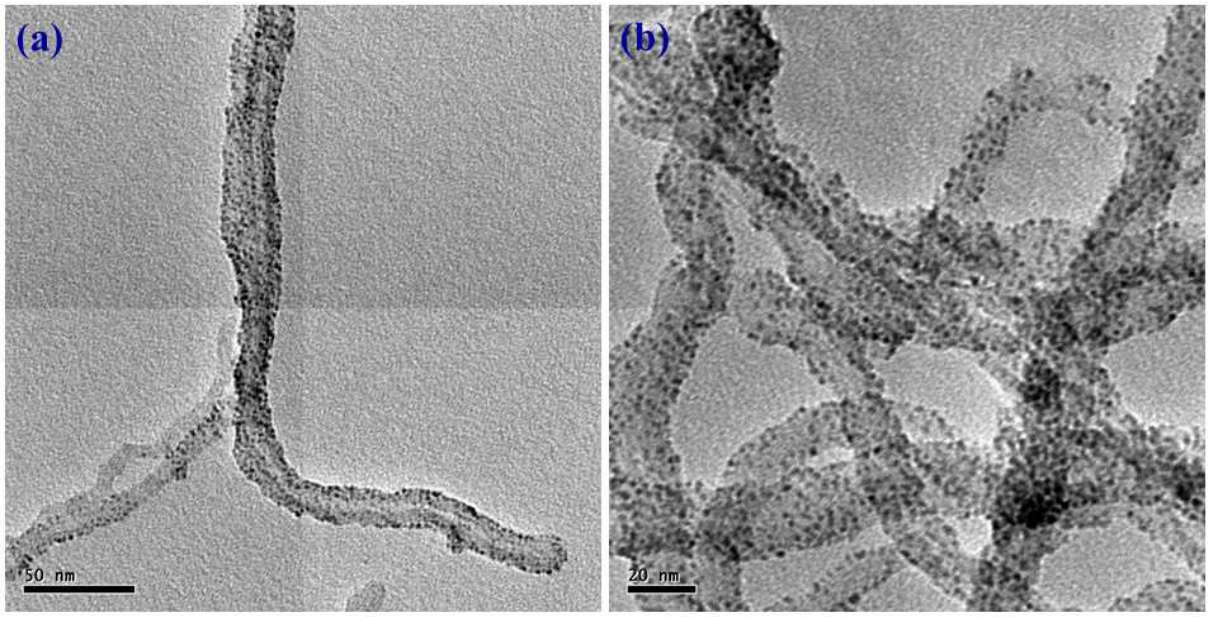

Figure 8 HRTEM images of (a) Pt/ATCP-CP-BZD-CNT and (b) Pt-Sn/ATCP-CP-BZD-CNT electrocatalysts.

HRTEM images of Pt/ATCP-CP-BZD-CNT and Pt-Sn/ATCP-CP-BZD-CNT were shown in the **Figure 8 (a &b)**. From the **Figure 8,** the shape, size and dispersion of metal nanoparticles on the surface of ATCP-CP-BZD-CNT composite was investigated. The TEM picture clearly demonstrates that the platinum and platinum-tin nanoparticles are spherical in shape and are uniformly deposited on the surface ATCP-CP-BZD-CNT composite. The average particle size of platinum and platinum-tin nanoparticles were found to be ~2.0 nm. The small size and uniform distribution of Pt and Pt-Sn nanoparticles were obtained due to the presence of three functional groups (i) -SO_3H groups (ii) -NH groups and (iii) -O groups

RSC Advances Accepted Manuscript

that are available on the surface of ATCP-CP-BZD-CNT composite (**scheme 1**). Further by comparing both the TEM images (Figures 7 and 8 (a&b) and XRD analysis, it was concluded that the most of the metal (Pt and Pt-Sn) nanoparticles were present on the surface of ATCP-CP-BZD but not on CNT.

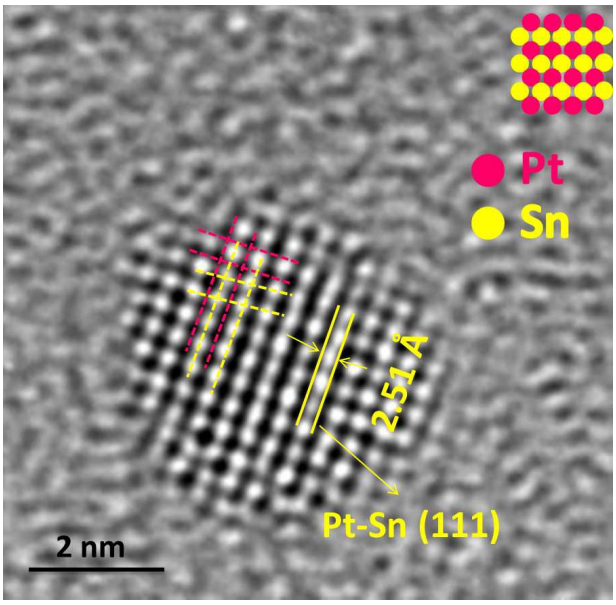

Figure 9 HRTEM image showing a single particle of Pt-Sn/ATCP-CP-BZD-CNT catalyst.

Additionally, the existence of Pt and Sn and their contact information on Pt-Sn/ATCP-CP-BZD-CNT catalyst was shown in **Figure 9**. The inter-planar distance (spacing) was measured for a particle present in the HRTEM picture and its value was 2.51 Å, which is corresponding to (111) plane of Pt-Sn bimetal present on ATCP-CP-BZD-CNT catalyst. Further, the existence of Pt and Sn and their contact information were visualized from the TEM picture (and insert picture) of Pt-Sn/ATCP-CP-BZD-CNT catalyst. Hence, the HRTEM image of the single particle (**Figure 9**) confirms the formation of Pt-Sn bimetal and their contact information on ATCP-CP-BZD-CNT surface during the formaldehyde reduction procedure.

RSC Advances Accepted Manuscript

Further, the EDX analysis confirms the existence of platinum and platinum-tin metal nanoparticles on ATCP-CP-BZD-CNT surface (**Figure 10 (a & b)**). The nominal and actual loading of mono and bi-metallic nanoparticles present on ATCP-CP-BZD-CNT composite was shown in the **Table 1**. Further, it affords supporting evidences for the existence of metal nanoparticles on ATCP-CP-BZD-CNT composite.

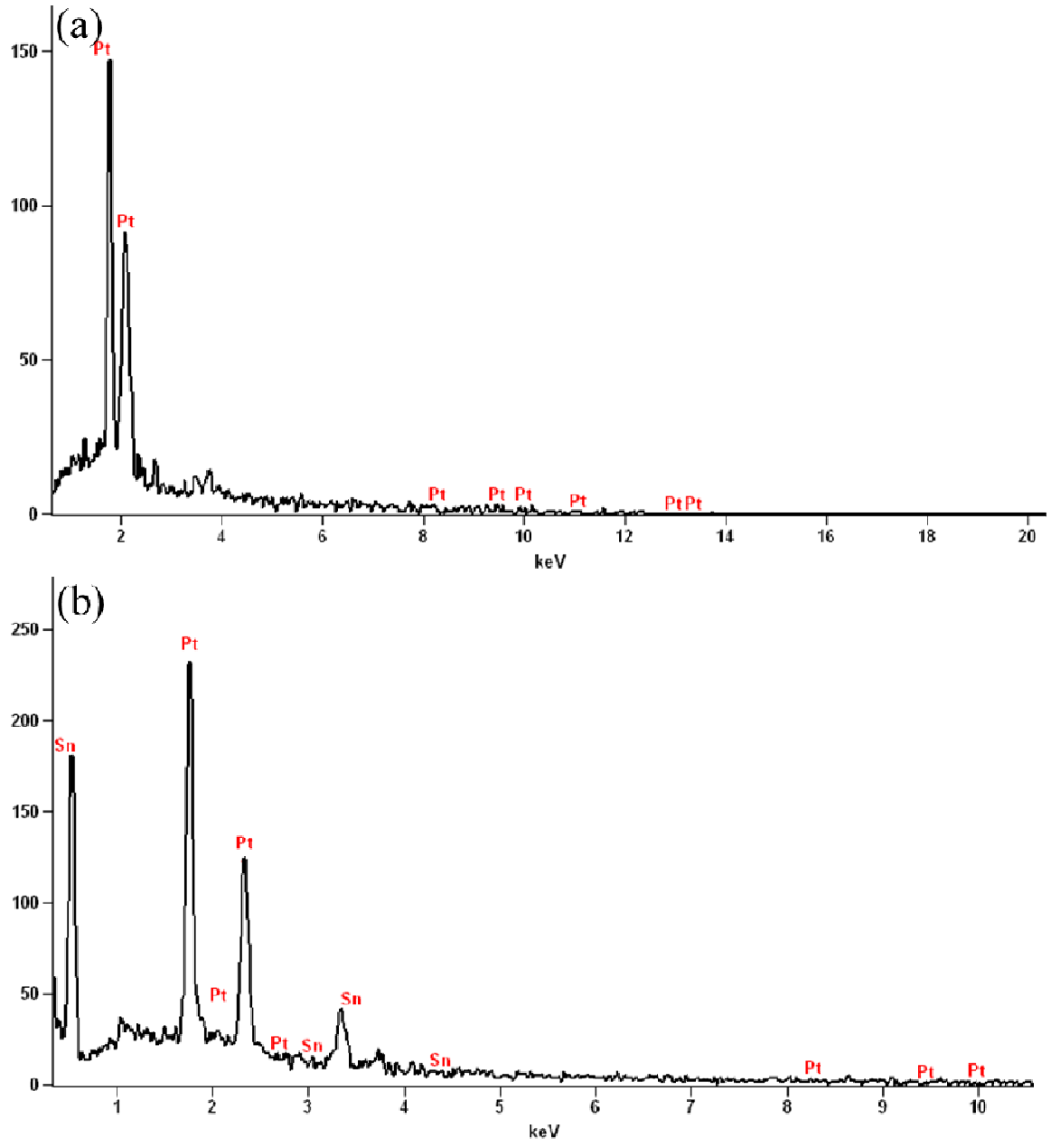

RSC Advances Accepted Manuscript

Figure 10 Energy dispersive X-ray analysis pattern of (a) Pt/ATCP-CP-BZD-CNT and (b) Pt-Sn/ATCP-CP-BZD-CNT composites

Table 1 Nominal and actual composition of the catalyst of metal nanoparticles obtained from EDX analysis

Sl.No.	Catalyst	Nominal composition (%)		Actual composition (%)	
		Pt	Sn	Pt	Sn
1	Pt/ATCP-CP-BZD-CNT	100	0	100	0
2	Pt-Sn/ATCP-CP-BZD-CNT	50	50	48.85	51.15

Electrooxidation of glycerol

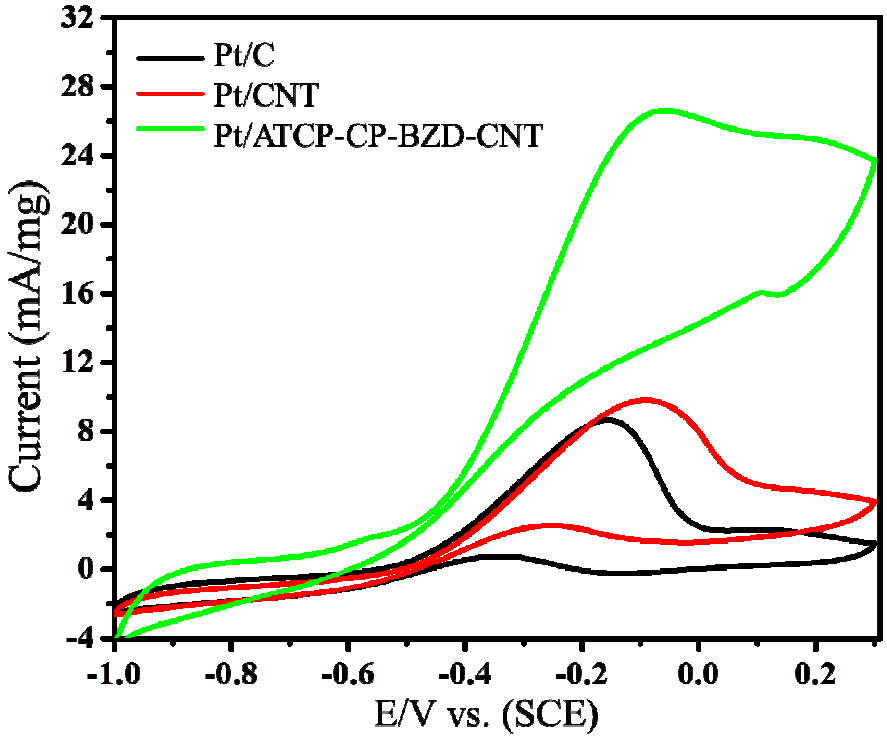

Figure 11 Cyclic voltammograms of Pt/C, Pt/CNT and Pt/ATCP-CP-BZD-CNT catalysts in 0.5 M KOH and 0.5 M glycerol solution at 50 mVs^{-1}.

Before the electrooxidation of glycerol on bimetallic system, it is necessary to study the effect of the support materials for electrocatalysis process. For this, the electrooxidations of glycerol were carried out on Pt/C and Pt/CNT along with Pt/ATCP-CP-BZD-CNT

RSC Advances Accepted Manuscript

catalysts in alkali medium. The cyclic voltammograms of Pt/C, Pt/CNT and Pt/ATCP-CP-BZD-CNT catalyst in 0.5 M KOH and 0.5 M glycerol solution are shown in **Figure 11**. From the **Figure 11,** it can be clearly seen that the glycerol oxidation peak was observed at -0.05 V vs. SCE for Pt/ATCP-CP-BZD-CNT electrode with the oxidation current of 26.59 mA/mg and it was considerably greater than that of the Pt/CNT and Pt/C, which might be due to the combined synergy effect of ATCP-CP-BZD and CNT in ATCP-CP-BZD-CNT material.

Further, in the present work three potent functional groups namely –NH, -SO_3H and –O were present on ATCP-CP-BZD-CNT novel support, which will favors more enhanced effect than that of any other doped material. Hence, the functionalized CNT has a positive influence on the nucleation growth and binding properties with metal nanoparticles, which will also result smaller particle size, better dispersion and a uniform size distribution. The good dispersion and distribution of the metal nanoparticle on support is one of the most basic features for an efficient catalyst , which lead to increase in the surface area of catalyst. Especially nitrogen doped CNT owns high surface nucleation sites, which allow the anchorage and high dispersion of the metal nanoparticles on the surface of supporting material that results in high interaction between nitrogen-doped CNT support and the catalytic metals[25-27]. Besides, nitrogen doped CNT can improve the durability of the CNT supported catalyst due to the strong interaction between the nitrogen doped CNT and metal nanoparticles, which is due to the electron donor behavior of nitrogen. So, nitrogen doped CNT can be employed as a high-efficiency electrocatalyst for fuel cell application.[26]

Generally, in the negative scan the oxidation of glycerol does not occur until the surface oxide are reduced, which results the reactivating of electrode surface for further

RSC Advances Accepted Manuscript

glycerol adsorption and electrooxidation[28]. The quasi-superimposition of the curves during the positive and the negative potential sweeps suggests the poisoning effects. Further, this will limit the rate of glycerol adsorption on Pt surface and hence electroxidation current decreases. From this literature observation, the present results conclude that there no such positive curves were observed during the negative sweep, which demonstrates the reduced poison effect on Pt/ATCP-CP-BZD-CNT anode catalyst.

From the literature reports[28,29] it has been noticed that the oxidation of glycerol on platinum surface yields intermediates such as glyceraldehyde, glyceric acid, glycolic acid and formic acid. Though other products are formed, formic acid plays an important role as it paves a way for the formation of poisonous intermediate CO(ads).[28-30] Hence, based on the present investigation results (HPLC results), the possible proposed mechanism was hypothesized for glycerol oxidation on Pt/ATCP-CP-BZD-CNT electrocatalyst (**Scheme 2**).

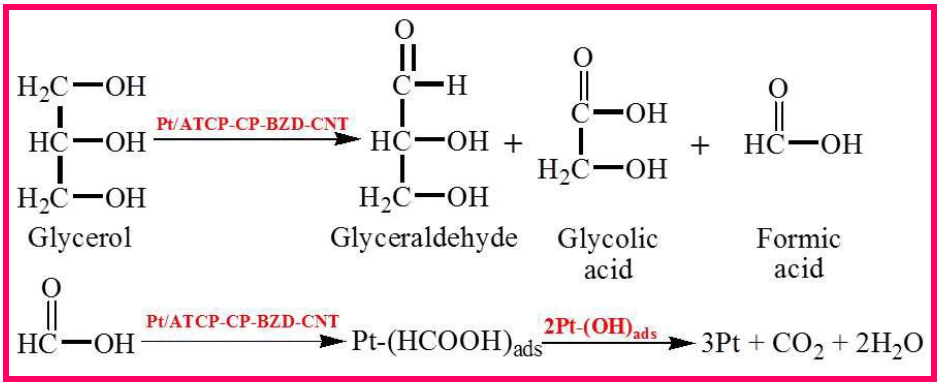

Scheme 2 Proposed mechanism based on the HPLC result for glycerol oxidation on Pt/ATCP-CP-BZD-CNT surface

During the oxidation of glycerol an evolution "CO_2" were noticed, which further support the mechanism[25]. From these studies, it could be understood that the formation of CO is vanished or not found on the surface of Pt/ATCP-CP-BZD-CNT electrode at lower

RSC Advances Accepted Manuscript

negative onset potential. So, the absence of CO can enhance the electrocatalytic activity of Pt/ATCP-CP-BZD-CNT electrode towards glycerol oxidation.

From the results, it has been noticed that the Pt/ATCP-CP-BZD-CNT catalyst exhibits higher electrocatalytic activity than that of the Pt/CNT and Pt/C catalysts in terms of onset potential and oxidation current. This indicates that the supporting material (ATCP-CP-BZD-CNT) plays an important in the electrooxidation of glycerol. Further, to enhance the catalytic activity and to reduce the cost of the electrode materials, platinum is alloyed with tin on ATCP-CP-BZD-CNT composite to form Pt-Sn/ATCP-CP-BZD-CNT electrocatalyst.

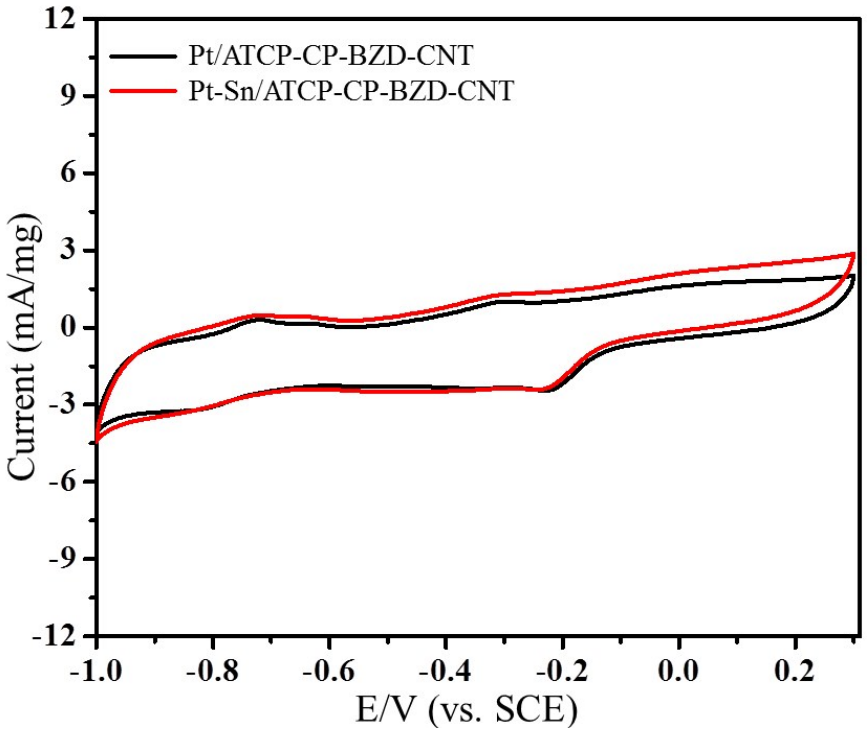

Figure 12 Cyclic voltammograms of Pt/ATCP-CP-BZD-CNT and Pt-Sn/ATCP-CP-BZD-CNT electrodes in 0.5 M KOH solution at a scan rate of 50 mVs^{-1}.

To compare the catalytic activity and stability of Pt/ATCP-CP-BZD-CNT with Pt-Sn/ATCP-CP-BZD-CNT as an anode catalyst, the electrooxidation of glycerol in 0.5 M

RSC Advances Accepted Manuscript

KOH solution was carried out by cyclic voltammetry and chronoamperometric techniques. **Figure 12** shows the cyclic voltammograms of Pt/ATCP-CP-BZD-CNT and Pt-Sn/ATCP-CP-BZD-CNT electrodes in 0.5 M KOH at a scan rate of 50 mVs^{-1}.

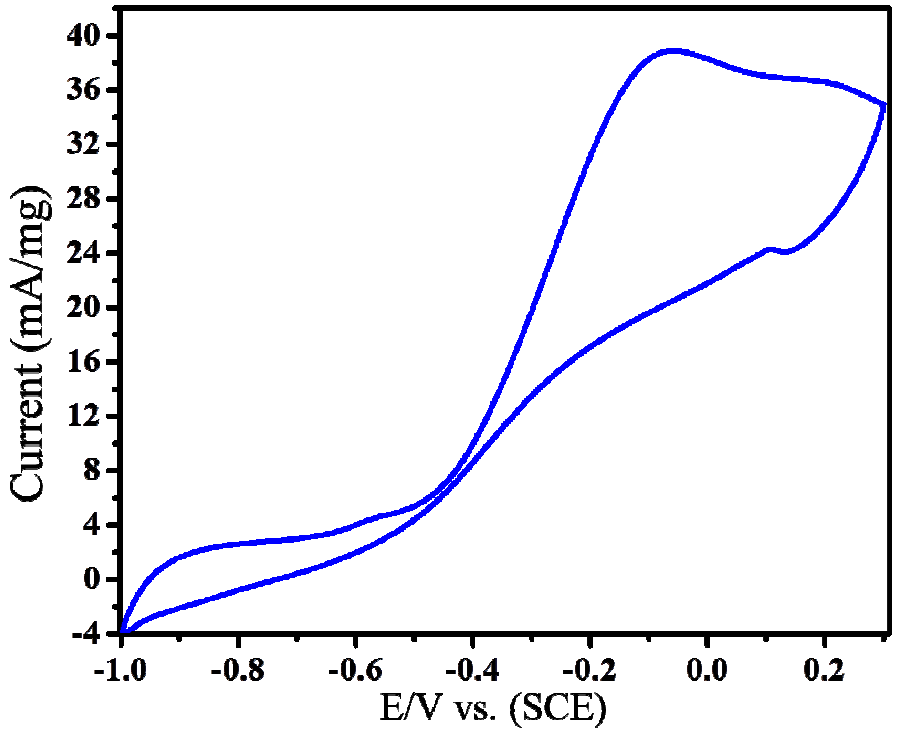

Figure 13 Cyclic voltammograms of Pt-Sn/ATCP-CP-BZD-CNT electrode in 0.5 M KOH + 0.5 M glycerol solution at a scan rate 50 mVs^{-1}.

From the **Figure 12**, it can be seen clearly that the oxidation peak was not observed for Pt/ATCP-CP-BZD-CNT and Pt-Sn/ATCP-CP-BZD-CNT electrodes in 0.5 M KOH solution. **Figure 13** depicts the cyclic voltammetric responses of Pt-Sn/ATCP-CP-BZD-CNT electrodes in 0.5 M KOH + 0.5 M glycerol solution at 50mVs^{-1}.

From the **Figure 13**, it was noticed that the presence of tin as second metal has shown remarkable effects towards glycerol oxidation. The enhanced glycerol oxidation peak current of Pt-Sn/ATCP-CP-BZD-CNT is 38.89 mA, which was higher than that of

RSC Advances Accepted Manuscript

Pt/ATCP-CP-BZD-CNT electrocatalyst (26.59 mA). Further, the reduced onset potential of Pt-Sn/ATCP-CP-BZD-CNT is -0.74 V, which was more negative than that of Pt/ATCP-CP-BZD-CNT electrocatalyst (-0.64 V). From the results, it has been concluded that the electrocataltytic activity of glycerol oxidation in the present study shows higher oxidation and lower onset potential than those of Pt/CNT and Pt/C electrocatalyst **(Figure 13)**. This enhanced catalytic activity and reduced poison effect may be due to the synergy effect among the metal (Pt and Pt-Sn) nanoparticles, ATCP-CP-BZD and CNT materials. From the results, it has been concluded that the prepared Pt/ATCP-CP-BZD-CNT and Pt-Sn/ATCP-CP-BZD-CNT are good and potent electrocatalyst for glycerol oxidation.

Chromatographic analysis of intermediate product formed during glycerol oxidation

The high performance liquid chromatography (HPLC) measurements were carried out to find the intermediate products formed during the electrooxidation of glycerol on Pt/ATCP-CP-BZD-CNT and Pt-Sn/ATCP-CP-BZD-CNT catalysts. The HPLC analysis evidences that both Pt and Pt-Sn nanoparticles present on ATCP-CP-BZD-CNT support are able to dissociate glycerol into fragments containing a single carbon at a high percentage under mild experimental conditions.

Figure 14 shows the chromatograms obtained from HPLC analysis during the electrooxidation of glycerol on Pt/ATCP-CP-BZD-CNT and Pt-Sn/ATCP-CP-BZD-CNT catalysts. The intermediate product formed during the electrooxidation of glycerol on Pt/ATCP-CP-BZD-CNT and Pt-Sn/ATCP-CP-BZD-CNT catalysts were obtained by HPLC analysis.

RSC Advances Accepted Manuscript

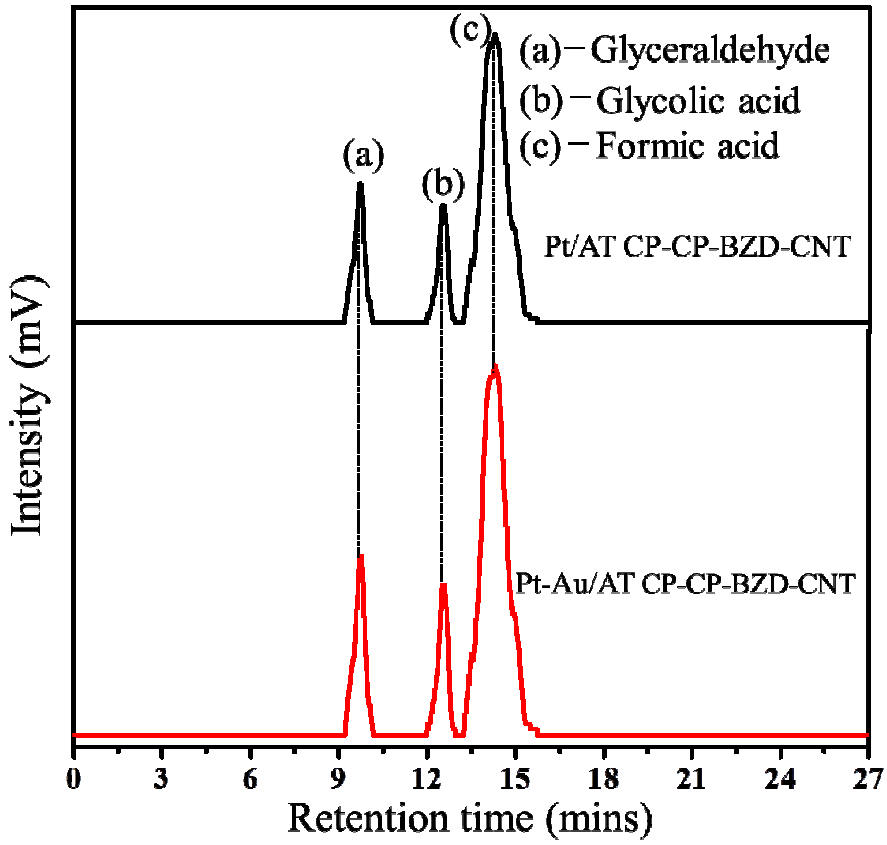

Figure 14 Chromatograms obtained from HPLC analysis during the electrooxidation of glycerol on Pt/ATCP-CP-BZD-CNT and Pt-Sn/ATCP-CP-BZD-CNT catalysts

Figure 15 shows the comparative bar graph of intermediates obtained during the electrooxidation of glycerol on Pt/ATCP-CP-BZD-CNT and Pt-Sn/ATCP-CP-BZD-CNT catalysts. The Pt/ATCP-CP-BZD-CNT catalyst exhibits 26.59 mA current for 4 hours and yielding 66% of formic acid, 20% of glyceraldehyde and 14% of glycolic acid. Similarly, Pt-Sn/ATCP-CP-BZD-CNT catalyst exhibits 38.89 mA current for the same 4 hours and yielding 70% of formic acid, 17% of glyceraldehyde and 13% of glycolic acid. Glycerol is first oxidized to form three intermediates namely glyceraldehyde, glycolic acid and formic acid. The formed glyceraldehyde and glycolic acid are oxidized and they undergo cleavage of C–C bond to produce CO_2 as a byproduct. Similarly, the formic acid gets oxidized to give

RSC Advances Accepted Manuscript

CO_2. Unfortunately, the HPLC is unable to identify the formation of CO_2 or carbonates.[32] However, the cyclic voltammograms of Pt/ATCP-CP-BZD-CNT and Pt-Sn/ATCP-CP-BZD-CNT catalysts (Figures 11 & 13) evidenced the absence CO poison on anode catalyst.[28] Hence, the above discussion gives clear information regarding the intermediate products formed during the glycerol oxidation process except CO_2 generations.

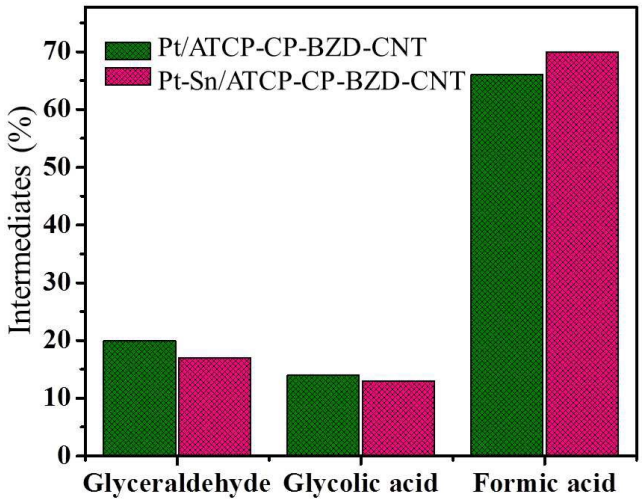

Figure 15 The comparative bar graph of intermediates produced during the electrooxidation of glycerol on Pt/ATCP-CP-BZD-CNT and Pt-Sn/ATCP-CP-BZD-CNT catalysts.

Effect of scan rates

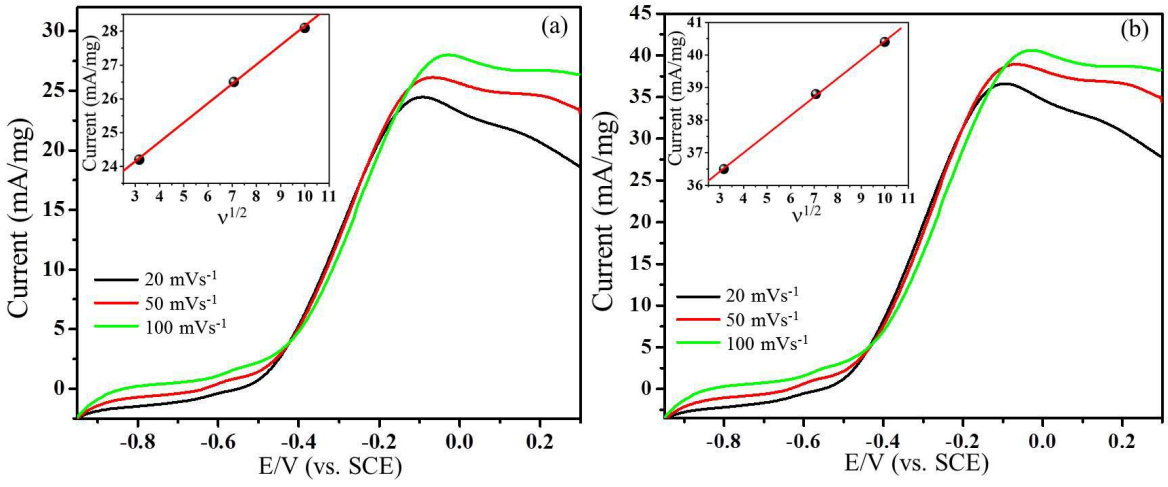

RSC Advances Accepted Manuscript

Figure 16 Effect of scan rate on (a) Pt/ATCP-CP-BZD-CNT (b) Pt-Sn/ATCP-CP-BZD-CNT nanocatalyst in 0.5 M KOH + 0.5 M glycerol (scan rate = 20, 50 and 100 mVs^{-1}). The inset image shows the dependence of the oxidation currents on the square root of scan rates.

The high performance of Pt/ATCP-CP-BZD-CNT and Pt-Sn/ATCP-CP-BZD-CNT modified electrodes make us to know the nature of mass transport behaviour of the alcohol. The forward cycle of cyclic voltammograms has been recorded at three different scan rates (20, 50 and 100 mVs^{-1}) in 0.5 M KOH + 0.5 M glycerol solution (**Figure 16 (a&b)**). **Figure 16** confirms that the oxidation current increases with an increase in the scan rates. The insert figure shows the plot between the oxidation current versus the square root of the scan rates that furnishes the linear relations with linear regression equation correlation coefficient values of 0.9995 and 0.9978 for Pt/ATCP-CP-BZD-CNT and Pt-Sn/ATCP-CP-BZD-CNT respectively, which are confirming the transport properties of glycerol. The above results concluded that the glycerol oxidation reaction is a diffusion-controlled reaction processes.[27]

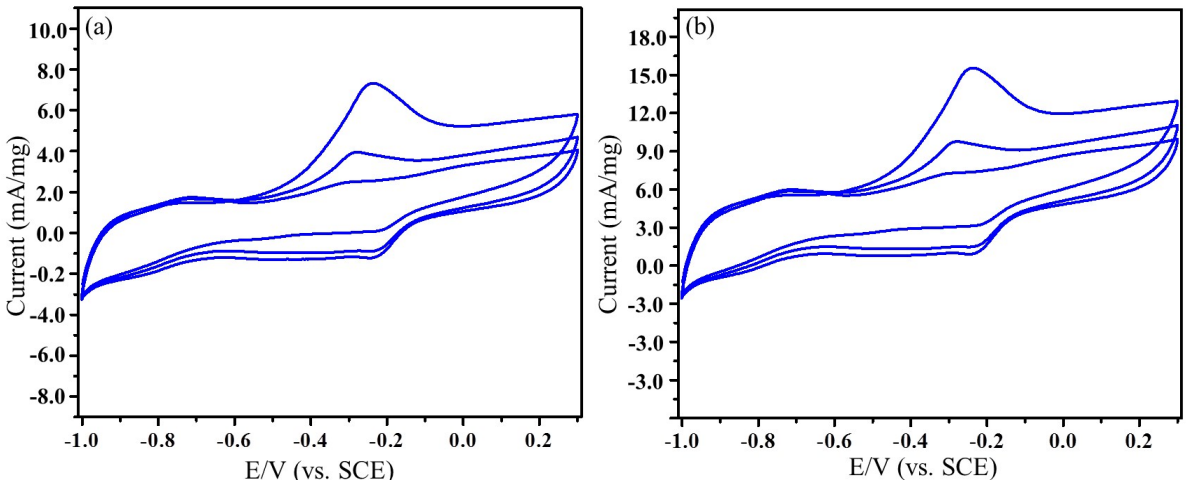

RSC Advances Accepted Manuscript

Figure 17 Cyclic voltammograms of (a) Pt/ATCP-CP-BZD-CNT (b) Pt-Sn/ATCP-CP-BZD-CNT electrodes in 0.5M KOH solution at a scan rate of 50 mVs^{-1} after electrooxidation of glycerol.

Furthermore, the adsorption and diffusion of the glycerol have been observed practically by carrying out the electrochemical measurement in 0.5 M KOH solution after carrying out the glycerol oxidation reaction. From the **Figure 17 (a & b),** the oxidation peak current is observed for first and second cycle of the voltammograms but in the third cycle no oxidation peak current has been observed. The results confirm the diffusion and adsorption of glycerol molecules on the surface of the Pt/ATCP-CP-BZD-CNT and Pt-Sn/ATCP-CP-BZD-CNT materials. Hence, this is also practically confirming that the electrooxidation of glycerol is diffusion-control process.

Effect of concentration of glycerol

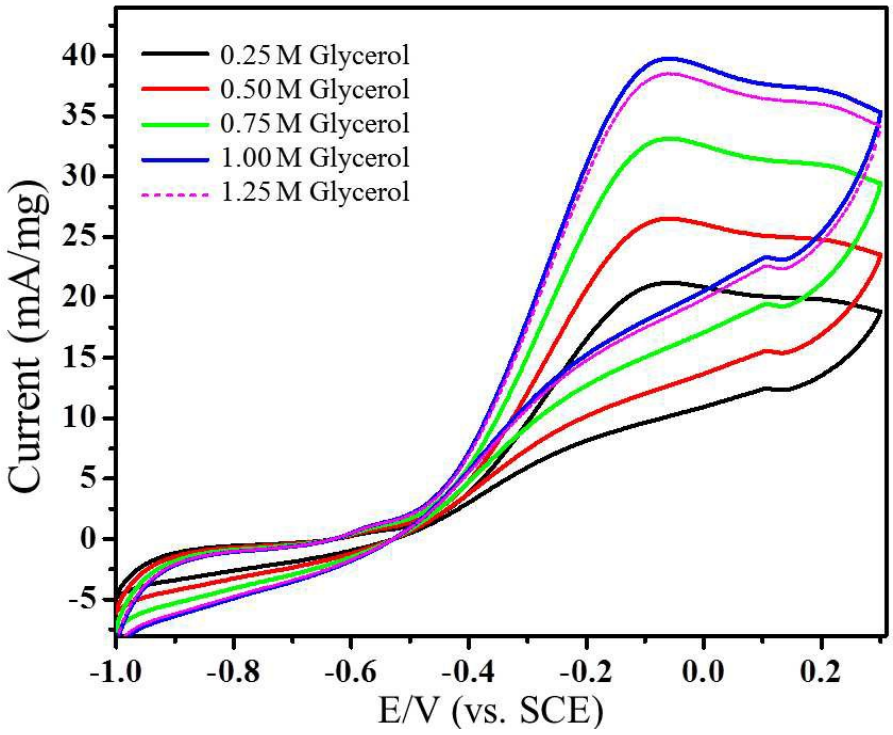

RSC Advances Accepted Manuscript

Figure 18 Effect of glycerol concentration in 0.5 M KOH solution on Pt/ATCP-CP-BZD-CNT catalyst

The effect of concentrations of glycerol (0.25, 0.50, 0.75, 1.00 and 1.25 M) on the surface of Pt/ATCP-CP-BZD-CNT electrode was carried out in 0.5 M KOH solution at a scan rate of 50 mV/s^{-1} **(Figure 18).** From the cyclic voltammogram, the oxidation peak current increases with the increase of glycerol concentration up to 1.00 M and decrease further increase in the concentration of glycerol. This can be attributed due to the saturation of active sites on Pt/ATCP-CP-BZD-CNT electrocatalyst with glycerol that hinders the OH adsorption on Pt sites, which is essential for the electrooxidation of glycerol. Hence, the decrease of oxidation peak current has been observed in the case of 1.25M glycerol solution.[31]

Chronoamperometric analysis

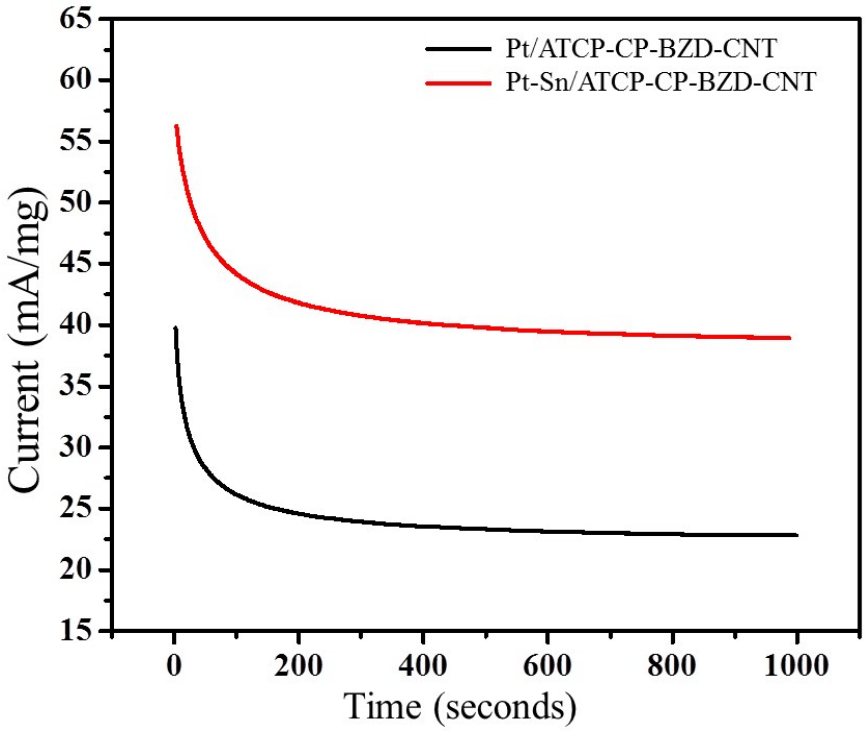

RSC Advances Accepted Manuscript

Figure 19 Chronoamperograms of Pt/ATCP-CP-BZD-CNT and Pt-Sn/ATCP-CP-BZD-CNT electrocatalysts in 0.5 M KOH and 0.5 M glycerol solution at a potential of $50mVs^{-1}$.

Figure 19 shows the chronoamperograms of Pt/ATCP-CP-BZD-CNT and Pt-Sn/ATCP-CP-BZD-CNT modified graphite electrodes in 0.5 M KOH + 0.5 M glycerol. From the **Figure 19,** it was noticed that the steady state current decrease initially, but after a few seconds the constant steady state current has been observed for Pt/ATCP-CP-BZD-CNT and Pt-Sn/ATCP-CP-BZD-CNT electrocatalysts. The decrease in the steady state current initially is due to the formation of double-layer charge and the carbonaceous intermediates on the surface of the electrode during the electrooxidation of glycerol.[33] The steady state current observed from chronoamperometric analysis is in good accord with the current observed from the cyclic voltammetry analysis.

From the chronoamperometric analysis, it was concluded that the Pt/ATCP-CP-BZD-CNT and Pt-Sn/ATCP-CP-BZD-CNT are good electrocatalysts with long term stability for the glycerol oxidation, which are due to small particle size, uniform distribution of metal nanoparticles on ATCP-CP-BZD-CNT composites and synergic effect among metal nanoparticls (Pt & Pt-Sn), ATCP-CP-BZD and CNT in Pt/ATCP-CP-BZD-CNT and Pt-Sn/ATCP-CP-BZD-CNT composites.

RSC Advances Accepted Manuscript

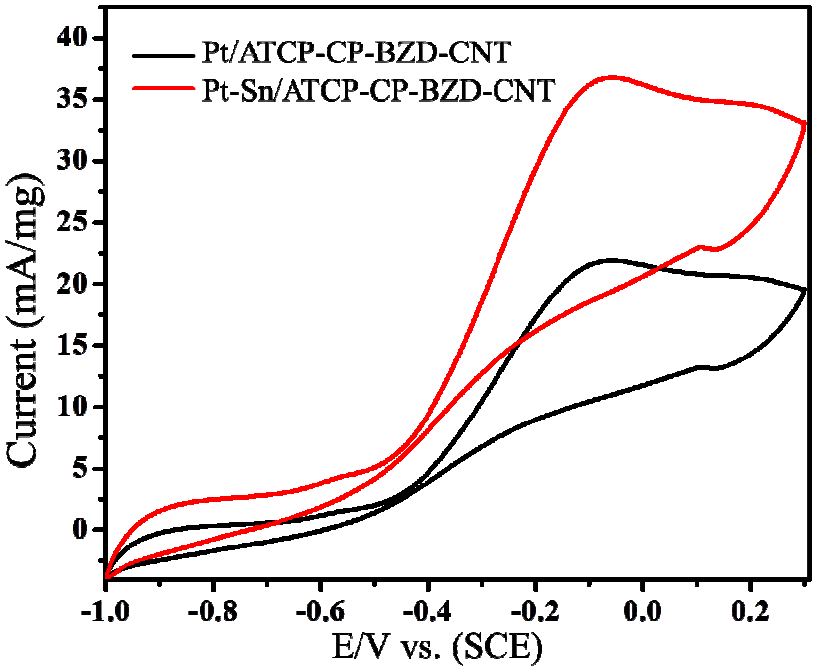

Figure 20 Electrooxidation of glycerol on used Pt/ATCP-CP-BZD-CNT and Pt-Sn/ATCP-CP-BZD-CNT electrodes at a scan rate 50 mVs^{-1}.

After the long-term CV experiments, the Pt/ATCP-CP-BZD-CNT and Pt-Sn/ATCP-CP-BZD-CNT electrodes were stored in double distilled water for a week and then the glycerol oxidation was carried out by using the same catalyst **(Figure 20)**. The results indicate that there is no significant changes were observed in the catalytic activity. This observation indicates that both the electrodes prepared in the present work have good long-term stability, storage properties and reusable capacity.

Conclusion

A novel ternary polymer-CNT (ATCP-CP-BZD-CNT) composite was prepared by a simple method at room temperature. Platinum and platinum-tin nanoparticles were deposited on ATCP-CP-BZD-CNT composite by the formaldehyde reduction method. ATCP-CP-BZD-CNT is a good support availing with three functional groups (-NH, -HSO_3

RSC Advances Accepted Manuscript

and -O), which are responsible for the uniform deposition of platinum and platinum-tin nanoparticles on ATCP-CP-BZD-CNT composite with the particle size of ~2.0 nm. From the electrochemical analyses, the Pt/ATCP-CP-BZD-CNT and Pt-Sn/ATCP-CP-BZD-CNT electrocatalyst exhibits high oxidation current (26.59 mA mg^{-1} of Pt and 38.89 mA mg^{-1} of Pt-Sn) at lower negative onset potential (-0.64 V of Pt and -0.74 V of Pt-Sn) than the Pt/C and Pt/CNT towards the electrooxidation of glycerol in an alkaline medium. Hence, Pt/ATCP-CP-BZD-CNT and Pt-Sn/ATCP-CP-BZD-CNT electrocatalyst can be used as a potential anode material for an alkaline direct alcohol fuel cells (ADAFCs), because of its excellent electrocatytic activity, stability and lower negative onset potential towards the oxidation of glycerol.

Acknowledgement

The authors like to thank DST/Nanomission, New Delhi, India for the financial support to carry out this work and the establishment of Nanotech Research Lab through the grant No. SR/NM/NS-05/2011(G).

Reference

1. Fashedemi, O.O.; Miller, H.A.; Marchionni, A.; Vizza F.; Ozoemen, K.I. Electro-oxidation of ethylene glycol and glycerol at palladium-decorated FeCo@Fe core–shell nanocatalysts for alkaline direct alcohol fuel cells: functionalized MWCNT supports and impact on product selectivity, *J. Mater. Chem. A,* **2015**, *3*, 7145-7156.
2. Xin, L.; Zhang, Z.; Wang Z.; Li, W. Simultaneous Generation of Mesoxalic Acid and Electricity from Glycerol on a Gold Anode Catalyst in Anion-Exchange Membrane Fuel Cells, *Chem.Cat.Chem,* **2012,** *4*, 1105-1114.

RSC Advances Accepted Manuscript

3. Zhang, Z.; Xin L.; Li, W. Electrocatalytic oxidation of glycerol on Pt/C in anion-exchange membrane fuel cell: Cogeneration of electricity and valuable chemicals, *Appl. Catal., B* **2012,** *119–120*, 40-48.
4. Gerpen, J.V. Biodiesel processing and production*, Fuel Process. Technol.,* **2005**, *86,* 1097-1107.
5. Iijima, S. Biodiesel processing and production, *Nature*, **1991**, *354*, 56-58.
6. Tans, S.J.; Verschueren A.R.M.; Dekker, C. Room-temperature transistor based on a single carbon nanotube, *Nature*, **1998**, *393*, 49-52.
7. Planeix, J.M.; Coustel, N.; Coq, B.; Brotons, V.; Kumbhar, P.S.; Dutartre, R.; Geneste, P.; Bernier P.; Ajayan, P.M. Application of Carbon Nanotubes as Supports in Heterogeneous Catalysis, *J. Am. Chem. Soc.,* **1994**, *116*, 7935-7936.
8. Maiyalagan, T. Synthesis and electro-catalytic activity of methanol oxidation on nitrogen containing carbon nanotubes supported Pt electrodes, *Appl. Catal., B* **2008**, *80*, 286-295.
9. Prabhuram, J.; Zhao, T.S.; Tang, Z.K.; Chen R.; Liang, Z.X. Multiwalled Carbon Nanotube Supported PtRu for the Anode of Direct Methanol Fuel Cells, *J. Phys. Chem. B*, **2006**, *110*, 5245-5252.
10. Wang, J.; Yin, G.; Shao, Y.; Wang Z.; Gao, Y. Investigation of Further Improvement of Platinum Catalyst Durability with Highly Graphitized Carbon Nanotubes Support, *J. Phys. Chem. C,* **2008**, *112*, 5784-5789.
11. Shao, Y.; Liu, J.; Wang Y.; Lin, Y. Novel catalyst support materials for PEM fuel cells: current status and future prospects, *J. Mater. Chem.,* **2009**, *19*, 46-59.

RSC Advances Accepted Manuscript

12. Yang, W.; Wang, X.; Yang, F.; Yang C.; Yang, X. Carbon Nanotubes Decorated with Pt Nanocubes by a Noncovalent Functionalization Method and Their Role in Oxygen Reduction, *Adv. Mater.,* **2008**, *20*, 2579-2587.
13. Wang, S.; Jiang S.P.; Wang, X. Polyelectrolyte functionalized carbon nanotubes as a support for noble metal electrocatalysts and their activity for methanol oxidation, *Nanotechnology*, **2008**, *19*, 265601.
14. Fu, J.; Huang, X.; Huang, Y.; Zhang J.; Tang, X. One-pot noncovalent method to functionalize multi-walled carbon nanotubes using cyclomatrix-type polyphosphazenes, *Chem. Commun.*, **2009**, 1049-1051.
15. Selvaraj V.; Alagar, M. Pt and Pt–Ru nanoparticles decorated polypyrrole/multiwalled carbon nanotubes and their catalytic activity towards methanol oxidation, *Electrochem. Commun.,* **2007**, *9*, 1145-1153.
16. Li, W.; Liang, C.; Zhou, W.; Qiu, J.; Zhou, Z.; Sun G.; Xin, Q. Preparation and Characterization of Multiwalled Carbon Nanotube-Supported Platinum for Cathode Catalysts of Direct Methanol Fuel Cells, J. Phys. Chem. B, 2003, **107**, 6292-6299.
17. Krishnadevi, K.; Nirmala Grace. A.; Alagar, M.; Selvaraj, V. Development of hexa (aminophenyl)cyclotriphosphazene-modified cyanate ester composites for high-temperature applications, *High Performance Polymers***, 2014,** *26*, 89-96.
18. Krishnadevi, K.; Selvaraj, V.; Prasanna . D. Thermal, mechanical and antibacterial properties of cyclophosphazene incorporated benzoxazine blended bismaleimide composites, *RSC Adv.,* **2015,** *5*, 913-921.

RSC Advances Accepted Manuscript

19. Krishnadevi. K.; Selvaraj. V. Development of halogen-free flame retardant phosphazene and rice husk ash incorporated benzoxazine blended epoxy composites for microelectronic applications, *New J. Chem.,* **2015,** *39*, 6555-6567.
20. Patterson, A.L. The Scherrer Formula for X-Ray Particle Size Determination, *Phys. Rev.,* **1939**, *56*, 978.
21. Benaissi. K.; Johnson. L.; Walsha D.A.; Thielemans. W. Synthesis of platinum nanoparticles using cellulosic reducing agents. *Green Chem.,* **2010**, *12*, 220-222.
22. Yang. W.; Ma. Y.; Tang. J.; X. Yang. Green synthesis" of monodisperse Pt nanoparticles and their catalytic properties, *Colloids Surf., A.,* **2007**, *302*, 628–633.
23. Zheng. L.; Xiong. L.; Sun. J.; Li. J.; Yang. S.; Xia. J. Capping agent free synthesis of PtSn bimetallic nanoparticles with enhanced electrocatalytic activity and lifetime over methanol oxidation, *Catal. Commun*., **2008,** *9*, 624–629.
24. Qian, J.; Wei, W.; Huang, X.; Tao, Y.; Chen K.; Tang, X. A study of different polyphosphazene-coated carbon nanotubes as a Pt–Co catalyst support for methanol oxidation fuel cell, *J. Power Sources,* **2012**, *210*, 345-349.
25. Selvaraj, V.; Alagar M.; Hamerton, I. Electrocatalytic properties of monometallic and bimetallic nanoparticles-incorporated polypyrrole films for electro-oxidation of methanol, *J. Power Sources,* **2006**, *160*, 940-948.
26. Gong, K.P.; Du, F.; Xia, Z.H.; Durstock M.L.; Dai, M. Nitrogen-Doped Carbon Nanotube Arrays with High Electrocatalytic Activity for Oxygen Reduction, *Science* **2009**, *323*, 760-764.

RSC Advances Accepted Manuscript

27. He, Z.; Chen, J.; Liu, D.; Zhou H.; Kuang, Y. Electrodeposition of Pt–Ru nanoparticles on carbon nanotubes and their electrocatalytic properties for methanol electrooxidation, *Diamond Relat. Mater.* **2004**, *13*, 1764-1770.

28. Roquet, L.; Belgsir, E.M.; Leger J.M.; Lamy, C. Kinetics and mechanisms of the electrocatalytic oxidation of glycerol as investigated by chromatographic analysis of the reaction products: Potential and pH effects, *Electrochim. Acta,* **1994**, *39*, 2387-2394.

29. Nirmala Grace A.; Pandian, K. Pt, Pt–Pd and Pt–Pd/Ru nanoparticles entrapped polyaniline electrodes – A potent electrocatalyst towards the oxidation of glycerol, *Electrochem. Commun.,* **2006**, *8*, 1340-1348.

30. Schell, M.; Xu, Y.; Zdraveski, Z. Mechanism for the Electrocatalyzed Oxidation of Glycerol Deduced from an Analysis of Chemical Instabilities, *J. Phys. Chem.,* **1996**, *100*, 18962-18969.

31. Habibi E.; Razmi, H. Glycerol electrooxidation on Pd, Pt and Au nanoparticles supported on carbon ceramic electrode in alkaline media, *Int. J. Hydrogen Energy*, **2012**, *37*, 16800-16809.

32. Wang. H.; Thia. L.; Li. N.; Ge. X.; Liu. Z.; Wang. X. Pd nanoparticles on carbon-nitide-graphene for the selective electro-oxidation of glycerol in alkaline solution, *ACS Catal.* **2015**, *5*, 3174-3184.

33. Oliveira. R.T.S.; Santos. M.C.; Nascente. P.A.P.; Bulhões. L.O.S.; Pereira. E.C. Nanogravimetric and Voltammetric Studies of a Pt-Rh alloy Surface and its Behavior for Methanol Oxidation, *Int. J. Electrochem. Sci.,* **2008**, *3*, 970-979.

RSC Advances Accepted Manuscript

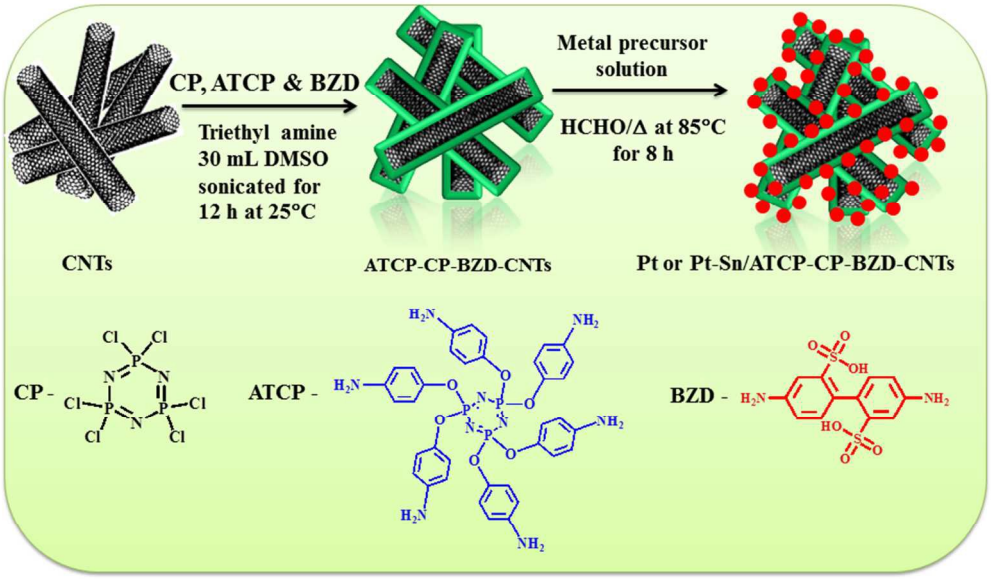

254x190mm (96 x 96 DPI)

RSC Advances Accepted Manuscript